Heliyon 10 (2024) e39071

Contents lists available at ScienceDirect

Heliyon

journal homepage: www.cell.com/heliyon

Research article

Shengqiyichang decoction regulates antitumor immunity in colorectal cancer by downregulating lymphocyte antigen 6 family member G6D via the protein kinase B/p38 mitogen-activated protein kinase signaling pathway

Run Xing Luo [a,1], Huai Liang Li [b,1], Yu Xiang Jia [a], Meng Gao [a], Zhao Yang Gao [a], Yi Ji [a], Shan Deng [a], Jie Ge Huo [a,*], Jian Zhang [a,b,**], Dong Jian Zhang [a]

[a] *Affiliated Hospital of Integrated Traditional Chinese and Western Medicine, Nanjing University of Chinese Medicine, Nanjing, 210028, Jiangsu Province, PR China*

[b] *Department of General Surgery, Lishui District Hospital of Traditional Chinese Medicine, Nanjing 211200, PR China*

ARTICLE INFO

Keywords:
Shengqiyichang decoction
Traditional Chinese medicine
Treg cells
Anti-tumor immunity
AKT/P38α signaling pathways

ABSTRACT

The traditional Chinese medicine (TCM) formulation Shengqiyichang Decoction (SQYCD) has been reported to stimulate host immunity, and it has been administered for the treatment of colorectal cancer (CRC). Here, we applied network and bioinformatics analyses to elucidate the mechanisms by which SQYCD ameliorates CRC and validated its modes of action via *in vivo* and *in vitro* experiments. We identified 46 active compounds in SQYCD and selected 237 proteins as potential therapeutic targets in CRC, most notably p38 mitogen-activated protein kinase (p38α). Bioinformatics analyses demonstrated differential expression in CRC tissues and prognostic value of the genes encoding TNFα, MAPK14, CASP-3, MAPK1, AKT1, PRKACA, VEGF, IL-6, EGFR and ESR1. We then plotted receiver operating curves (ROC) and time-ROC for the differentially expressed genes (DEGs) *ESR1* and *AKT1* to predict the progress of CRC. We speculated that the AKT/p38α-MAPK signaling pathway is associated with the clinical prognosis of CRC. In a mouse model, we found that SQYCD inhibits CRC tumor growth by increasing $CD4^+$ and $CD8^+$ T cell abundance and decreasing the ratio of T-regulatory cells (Tregs) in the tumor microenvironment. In cultured mouse CRC cells, SQYCD selectively upregulated levels of the CRC-associated protein lymphocyte antigen 6 family member G6D, while the AKT activator SC-79 reversed this effect. The discoveries made herein suggest that SQYCD exerts a therapeutic effect in CRC by inhibiting Treg recruitment via inhibition of the AKT/p38α/LY6G6D signaling axis.

* Corresponding author. Affiliated Hospital of Integrated Traditional Chinese and Western Medicine, Nanjing University of Chinese Medicine, Nanjing 210028, Jiangsu Province, PR China.

** Corresponding author. Affiliated Hospital of Integrated Traditional Chinese and Western Medicine, Nanjing University of Chinese Medicine, Nanjing 210028, Jiangsu Province, PR China.

E-mail addresses: huojiege@jsatcm.com (J.G. Huo), zhangjian@jsatcm.com (J. Zhang).

[1] These authors contributed equally to the work as co-first authors.

https://doi.org/10.1016/j.heliyon.2024.e39071
Received 2 April 2024; Received in revised form 3 September 2024; Accepted 7 October 2024
Available online 9 October 2024

1. Introduction

Colorectal cancer (CRC) is the third most prevalent type of cancer worldwide [1]. Annually, approximately 1.8 million new cases of CRC are identified, resulting in more than 800,000 related deaths [2]. Approximately 95 % of all CRC cases are the microsatellite-stable (MSS) form, which is characterized by an immune-excluded and immune-desert tumor microenvironment (TME), minimal tumor lymphocyte infiltration, and low tumor mutational burden [3]. Though chemotherapy remains the cornerstone of clinical CRC treatment, most therapeutic modalities have limited efficacy against the MSS type. In addition, MSS CRC is considered a "cold" cancer as it only weakly responds to immunotherapy. Consequently, innovative therapeutic strategies against MSS CRC are urgently needed [4]. Microsatellite or epigenetic instability may be critical in the pathogenesis of MSS CRC [5].

The immune response in the context of MSS CRC is typically weak, due to the presence of only low levels of $CD8^+$ and $CD4^+$ T cells [6]. Normally, $CD8^+$ T cells drive immune responses, particularly in the context of tumor immunity [7]. When antigen-presenting cells (APCs) present antigenic peptides and activate $CD8^+$ T cells via major histocompatibility complex class I (MHC-I), the $CD8^+$ T cells differentiate into cytotoxic effector T cells that directly kill their target cells. In contrast, $CD4^+$ T cells modulate immune responses by releasing cytokines that summon other immune cells to target sites, and they collaborate with dendritic cells to activate $CD8^+$ T cells [8]. When a TME lacks these two types of T cells, the tumor remains unchecked by the immune system, leading to more rapid growth and spread.

According to The Cancer Genome Atlas (TCGA) database, regulatory T cells (Tregs), abound in MSS CRC but not in CRC that is associated with microsatellite instability (MSI) [9]. Tregs suppress the activity of macrophages as well as T cells, B cells, natural killer cells, and dendritic cells. Therefore, Tregs are essential for shaping the tumor immune microenvironment [10]. Increased expression of the CRC antigen lymphocyte antigen 6 family member G6D (LY6G6D) is associated with increased infiltration of Tregs and other immune suppressor cells, and it plays an important role in inhibiting antitumor immunity [11]. LY6G6D-positive cells are more prevalent in CRC cells than in normal mucosa, and LY6G6D is markedly upregulated in MSS CRC compared to MSI CRC [12]. The protein p38α may modulate LY6G6D expression [13], and protein kinase B (AKT), which is upstream of p38α in a signaling axis, influences tumor growth, autophagy, immunity, and apoptosis [14–18]. For these reasons, we reasoned that targeting the AKT/p38α pathway and downregulating LY6G6D is a potential strategy to treat MSS CRC.

Chinese herbal medicine (CHM) has been a cornerstone of healthcare in China for millennia, and these medicines have been administered as adjunctive treatments for various complex disorders, including cancers [24]. For example, Sijunzi, Gegen Qinlian, and Chang Wei Qing decoctions have shown promise in the management of CRC when they are co-administered with immune checkpoint inhibitors. Shengqiyichang decoction (SQYCD) exhibits immunomodulatory activity and has been suggested to be a putative therapeutic agent against MSS CRC [25]. It was shown to increase the abundance of $CD4^+$ and $CD8^+$ T cells within tumor tissues [26].

SQYCD is a widely used traditional Chinese herbal formula that is composed of 6 medicinal herbs: *Panax ginseng* C. A. Mey (ren shen), *Actinidia chinensis* Planch (teng li gen), *Hedysarum multijugum Maxim* (huang qi), *Akebiae Fructus* (yu zhi zi), *Coicis Semen* (yi yi ren), and *Sophora flavescens Radix* (ku shen) in the ratio 10:15:15:10:20:6. Our systematic review and meta-analysis demonstrated that SQYCD herbs improve quality of life, relieve symptoms, and reduce adverse events in advanced CRC patients receiving chemotherapy [39]. A clinical study found that SQYCD improved the quality of life of CRC patients by reducing the adverse effects of conventional treatments and by improving outcomes when administered in combination with other treatments [25]. In this study, patients' clinical symptoms were found to improve significantly with co-administration of SQYCD, levels of immunological markers, including T-lymphocyte typing, were increased, and the frequency of leukopenia was reduced [25].

The present study applied network analysis and bioinformatics to investigate the mechanisms by which SQYCD exerts a therapeutic effect in the context of CRC. We also explored the therapeutic mode of action of SQYCD in a xenograft mouse model, and we clarified the anti-CRC mechanism of SQYCD on a molecular level using the murine CRC cell line CT-26.

2. Materials and methods

2.1. Animals

Male BALB/C mice, weighing 18 ± 2 g (Shanghai Jiesijie Company, Shanghai, China) were maintained in a controlled environment with a temperature of 25 ± 2 °C and a 12-h light/dark cycle. The mice received a standard diet and had ad libitum access to drinking water. All animal procedures adhered to national and international guidelines. Animal protocols were approved by the Jiangsu Province Academy of Traditional Chinese Medicine (SYXK (Su)K2021-0025), and the Animal Ethical Committee of the Jiangsu Province Academy of Traditional Chinese Medicine endorsed all animal experiments (AEWC-20210321-287).

2.2. Preparation of drugs

The Jiangsu Hospital of Traditional Chinese and Western Medicine provided the following herbal materials: *Panax ginseng* C. A. Mey (ren shen), *Actinidia chinensis* Planch (teng li gen), *Hedysarum multijugum* Maxim (huang qi), Akebiae Fructus (yu zhi zi), Coicis Semen (yi yi ren), and *Sophora flavescens* Radix (ku shen). The formulated granules were ground into a powder and dissolved in warm distilled water before administering to mice.

2.3. Prediction of pathways involved in anti-tumor activity of SQYCD based on network analysis

In the Traditional Chinese Medicine Systems Pharmacology Database and Analysis Platform (TCMSP) platform, a search was conducted for the effective ingredients of *Panax ginseng* C. A. Mey (ren shen), *Actinidia chinensis* Planch (teng li gen), *Hedysarum multijugum* Maxim (huang qi), Akebiae Fructus (yu zhi zi), Coicis Semen (yi yi ren), and *Sophora flavescens* Radix (ku shen), which are components of the SQYCD. The active components of SQYCD were searched, and the active components and drug targets were screened with oral bioavailability (OB) $\geq$ 30 % and DL $\geq$ 0.18. The gene names of the targets were identified using the Uniprot protein database and literature searches.

The GeneCards database (https://www.genecards.org/) was searched using "colorectal cancer" as a keyword to retrieve known targets involved in the pathogenesis of CRC. The targets of the drug ingredients and the disease targets were imported into the Venny2.1.0 analysis tool to generate a Venn diagram illustrating drug-disease common targets. The compound-target network for SQYCD and a protein-protein interaction (PPI) network were constructed and visualized using Cytoscape v. 3.5.1 (https://cytoscape.org/). Pathways interacting with the chosen targets were subsequently examined via gene ontology (GO) and Kyoto Encyclopedia of Genes and Genomes (KEGG) pathway enrichment analyses, using the criterion $P < 0.01$.

2.4. Bioinformatics analyses

The expression levels of the network core genes were extracted from the transcriptome data of the TCGA database. A heat map displaying gene expression levels in tumor and normal groups was drawn, as was a gene expression association map. The prognostic significance of these pivotal genes was statistically validated using univariate Cox regression analysis, adopting a significance threshold of $P < 0.05$. Kaplan-Meier survival curves were used to assess the predictive capabilities of pertinent risk genes. To ascertain the model's predictive precision, receiver operating characteristic (ROC) and time-ROC curves were formulated using the R packages timeROC, survival, and survminer. Correlations among the pivotal genes of the network were validated by inspecting a correlation scatter plot, accepting $P < 0.05$ as the threshold for statistical significance.

2.5. Molecular docking

Three-dimensional structures of target proteins were retrieved from the RCSB Protein Data Bank (http://www.pdb.org/). As a molecular visualization tool, PyMOL perform operations such as removing water molecules, adding hydrogen atoms, and correcting missing residues on the protein structure in preparation for subsequent molecular docking analysis. The three-dimensional chemical structures of the primary drug components were obtained from PubChem. Following the addition of hydrogen atoms and performing of charge calculations, Autodock Vina 1.1.3 was used to dock the compound with the primary targets, designating a binding energy of less than -5.0 kcal mol^{-1} as indicative of a stable binding site.

2.6. Creation and analysis of an in vivo model

To establish a tumor growth model, mice were subcutaneously injected with a 100 μL suspension of CT-26 cells (1×10^6 cells/mL). The body weights of the mice were monitored daily, and tumor volumes were gauged every 3 d using formula $(A \times B^2)/2$, where A is the tumor length and B is the tumor width. When the tumor volumes reached 50–150 mm^3, the mice were segregated randomly into 4 groups, with 6 mice in each group. Each group received varying doses of SQYCD and an anti-mouse CTLA4 antibody through intraperitoneal administration. SQYCD was administered daily, whereas the anti-CTLA4 antibody was administered tri-weekly for duration of 15 d. The dosages of SQYCD, 111 mg and 27 mg, were determined by converting moderate clinical doses into mouse equivalents. The anti-CTLA4 was administered at 0.2 mg. All control groups were administered an equivalent volume of vehicle (normal saline).

2.7. In vitro analysis of SQYCD cytotoxicity

CT-26 cells were cultured in RPMI 1640 medium, supplemented with 10 % fetal bovine serum (FBS; Zhejiang Tianhang Biotechnology, Hangzhou, China) and 100 μg/mL of 100 μg/mL penicillin and 100 μg/mL streptomycin. Cells were cultured at 37 °C in a humidified incubator with 5 % CO_2. Cells were treated with SQYCD (250–2000 μg/mL) for 24, 48, 72 h and then analyzed by the CCK-8 assay. Briefly, CCK-8 reagent (20 μL; Tsbiochem, Ltd., Shanghai, China) was added, and after a further incubation at 37 °C for 3 h, the absorbance at 450 nm was measured. The experiments were performed in triplicate.

2.8. Hematoxylin-eosin staining

Mouse tumor, liver, and kidney tissues were fixed with 4 % paraformaldehyde and then embedded in paraffin. Sections were then stained with hematoxylin and eosin (HE).

2.9. Immunohistochemistry

Tumor tissue sections fixed with paraformaldehyde were incubated with primary antibodies against FOXP3, CD4, CD8, LY6G6D, or antigen Kiel 67 (Ki-67) (Cell Signaling Technology, Beverly, MA, USA) at 37 °C for 2 h and then secondary antibody HPR anti-mouse or

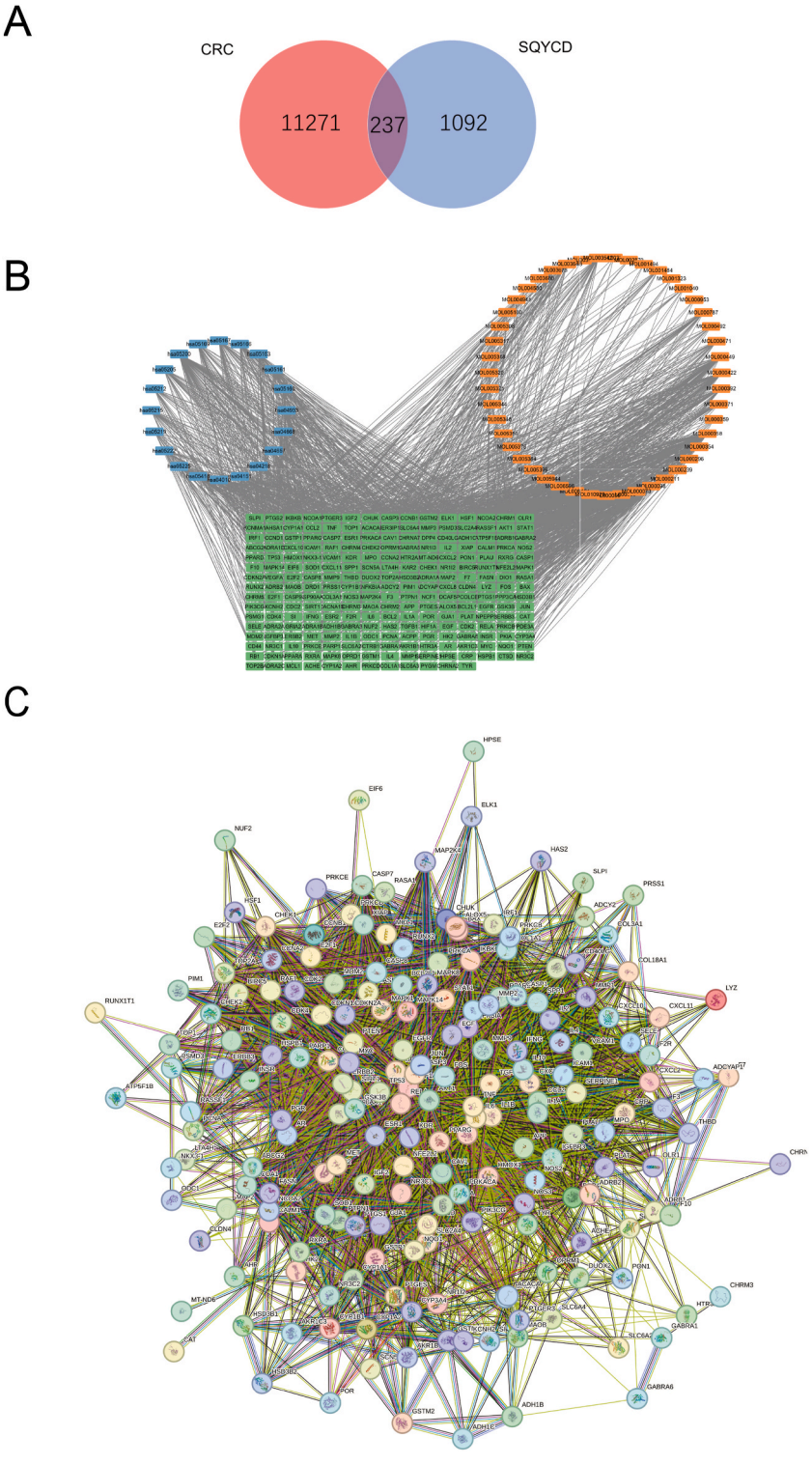

Fig. 1. Network Pharmacology diagram of SQYCD for the treatment of CRC (A)SQYC decoction active ingredient-target network. (B) The PPI network of 237 central genes targeted by SQYCD in CRC. (C) The PPI diagram features a circle representing one gene, with the protein structure at the center of the circle.

rabbit IgG (Maxim). The slides were colored with 3, 3'- Diaminobenzidine (DAB, Sigma-Aldrich) and counterstained by hematoxylin. The sections were rinsed three times with PBS. Protein expression was measured as positively stained area using Image-Pro.

2.10. Flow cytometry

All mice were instantly sacrificed before the spleens and tumors were harvested and blood was collected. The spleens and tumors were cut intom pieces and minced. Red blood cells (RBCs) were depleted using a RBC lysis solution (155 mmol L–1 NH4Cl, 10 mmol L–1 KHCO3,0.11 mmol L–1 EDTA.Na2,pH 7.2). Anticoagulated blood was obtained and the circulating immune cells were isolated by depleting the RBCs as described above. The immune cells were adjusted to 107 cells mL–1 and stained for 15 min in the dark with Zombie NIR™ FixableViability dye (Biolegend#423106), which dist inguishes live and dead cells since it is non-permeable to live cells, but permeable to the cells with compromised membranes. The cells were then pre-incubated with an anti-mouse CD16/32 antibody (Biolegend#101310) for 5–10 min on ice to block the non-specific binding of immunoglobulins to Fc receptors. A total of 106 cells in 100 μL were incubated with the following specific antibodies or isotype-matched controls at the manufacturers' recommended concentrations at 4 °C for 30 min. The labelled cells were then washed twice with PBS and reserved for flow cytometric analysis.The ratios of $CD3^+$ $CD4^+$, $CD3^+$ $CD8^+$, and $CD4^+$ $CD25^+$ $FOXP3^+$ cells in the spleens and tumor tissues of model mice were determined using flow cytometry. Prior to flow cytometric analysis, cells were incubated with the antibodies anti-mouse CD3-APC, anti-mouse CD4-FITC, anti-mouse CD8-PE, anti-mouse CD25-APC, and anti-mouse FOXP3-PE (Katimes Biotechnology, Hangzhou, China).

2.11. Western blot assay

Proteins were extracted from the tumor tissues or cultured cells, separated using SDS-PAGE, and transferred to polyvinylidene difluoride membranes. The membranes were blocked with 5 % bovine serum albumin for 2 h before being incubated overnight at 4 °C with primary antibodies against LY6G6D, p38α, phospho-p38α, AKT, phospho-AKT, and GAPDH (Abacam, Shanghai, China). In some cases, cells were treated with Sc-79, an AKT activator (Medchemexpress, Shanghai, China). The membranes were washed and then incubated with horseradish peroxidase-conjugated secondary antibodies (Beyotime Technology, Shanghai, China) for 1 h at 4 C. Signal was developed using enhanced chemiluminescent reagent (source) and was visualized using Image Studio, version 3.1.4.

2.12. ELISA

The serum levels of IL-10, IL-6, IL-2 and interferon (INF)-γ were quantified using ELISA kits (Beyotime Technology, Shanghai, China), following the manufacturer's instructions.

2.13. Statistical analysis

Statistical significance was established at a P-value of less than 0.05. Differences between two groups were compared using independent two-sample tests, employing a two-tailed Student's t-test and one-way ANOVA. Analyses were conducted using GraphPad Prism 8.

3. Results

3.1. Mechanisms and molecular targets of SQYCD in the treatment of CRC

Analyzing the compounds in SQYCD using the TCMSP database (OB $\geq$ 30 % and DL $\geq$ 0.18) led to the identification of 109 bioactive compounds and 1092 potential target proteins. In a separate analysis, we identified 11,271 potential target proteins in CRC using the GeneCards database. These targets were filtered, and duplicates were removed, and a resulting Venn diagram revealed 237 targets common to both SQYCD and CRC (Fig. 1A). These 237 genes corresponded to 46 active compounds in SQYCD.

We next constructed a compound-disease-target network with Cytoscape to depict the links among the 46 active compounds in SQYCD and the 237 potential disease targets. Based on centrality measurements, we identified quercetin, kaempferol, luteolin, β-sitosterol, taxifolin, and apigenin as the top six core compounds considered to have putative anti-CRC efficacy (Fig. 1B). The compound-disease-target network (Fig. 1B) displays candidate protein targets, the relevant active components, and the pathways where SQYCD is predicted to exert its effects.

A high-confidence PPI network generated using a minimum required interaction score of greater than 0.700 had 208 nodes, 856 edges, and an average node degree of 8.23. The mapped proteins were imported into Cytoscape to calculate the interaction network topological parameters for key proteins. By screening proteins with a degree score of more than 30, we selected the top ten priority targets: tumor necrosis factor-alpha (TNF-α), mitogen-activated protein kinase 14 (MAPK14), cysteinyl aspartate protease 3 (caspase-3; CASP3), MAPK1, protein kinase B1 (AKT1), cAMP-activated protein kinase catalytic subunit-alpha (PRKACA), vascular endothelial growth factor-alpha (VEGFA), interleukin 6 (IL-6), epidermal growth factor receptor (EGFR), and estrogen receptor 1 (ESR1) (Fig. 1C–Supplementary Table 1).

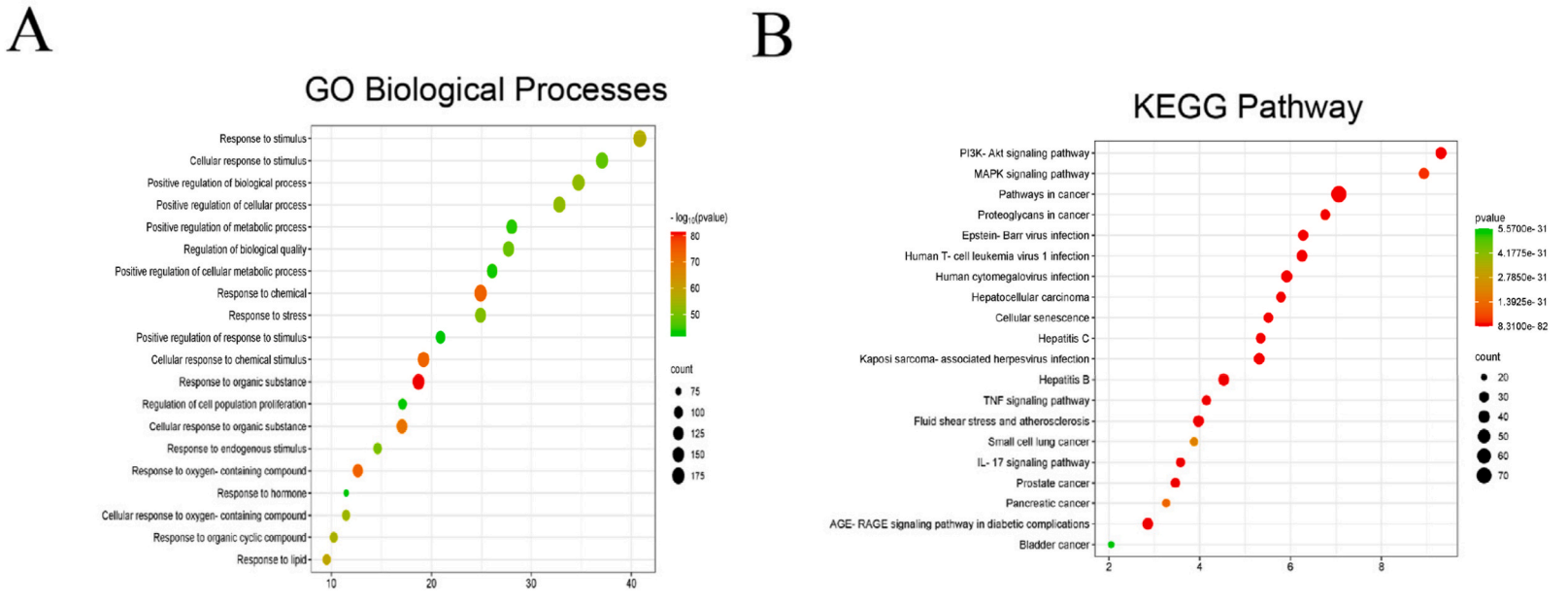

Fig. 2. The results of Gene Ontology Enrichment Analysis (A) The results of GO Enrichment Analysis. (B) The results of KEGG Enrichment Analysis.

3.2. GO and KEGG enrichment analyses

We subjected the targets of SQYCD to GO and KEGG pathway enrichment analyses to elucidate the molecular mechanisms of the therapeutic efficacy against CRC. We discovered that SQYCD may affect CRC via several biological processes, including response to stimulus, cellular response to stimulus, and positive regulation of biological and cellular processes (Fig. 2A). The MAPK, phosphoinositide-3-kinase enhancer (PI3k)/AKT, and IL-17 signaling pathways might mediate the therapeutic efficacy of SQYCD

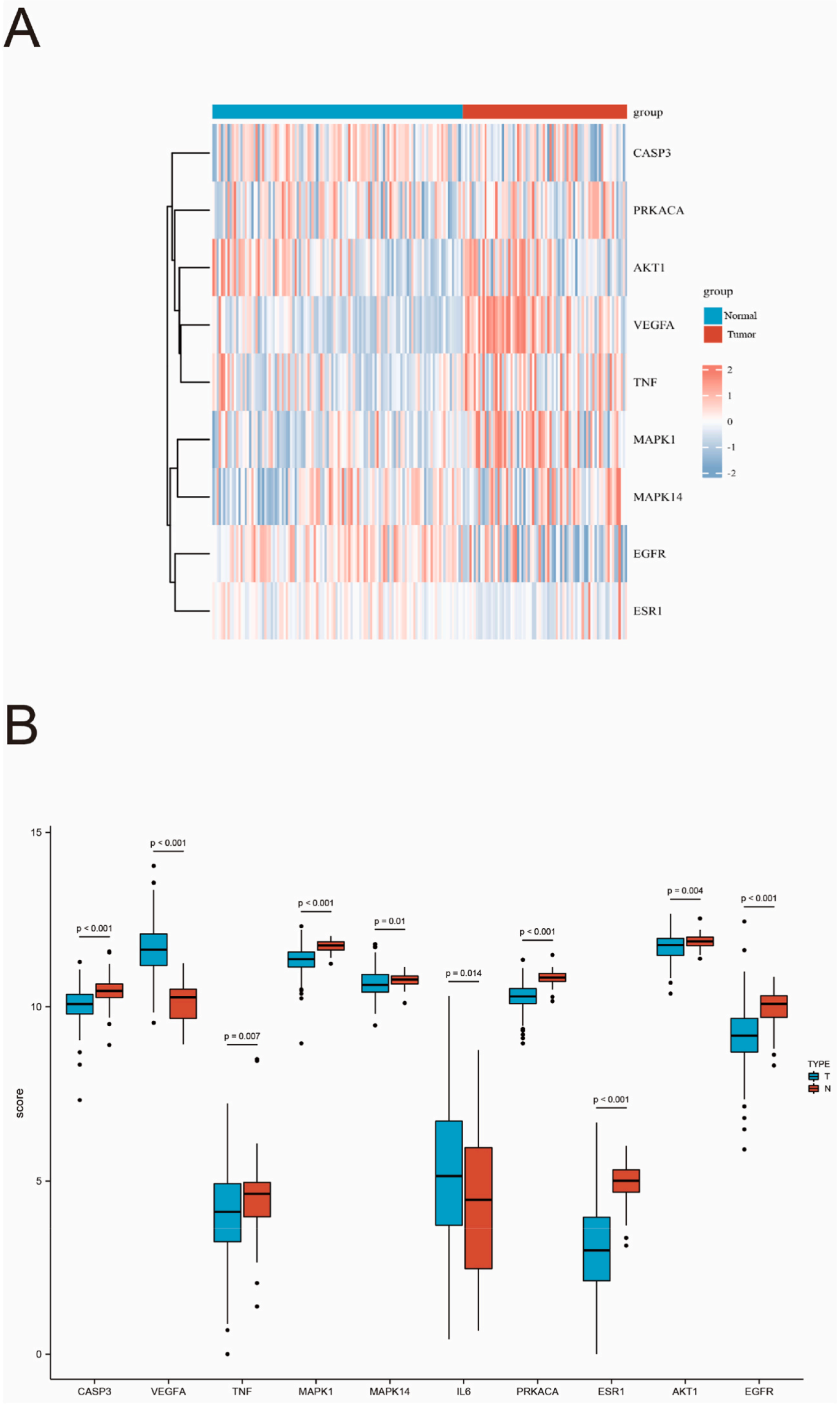

Fig. 3. Heatmap and Box diagram of network core gene expression in the TCGA database. (A) Heatmap of network core gene expression in the TCGA database. (B) Box diagram of differential expression of network core genes.

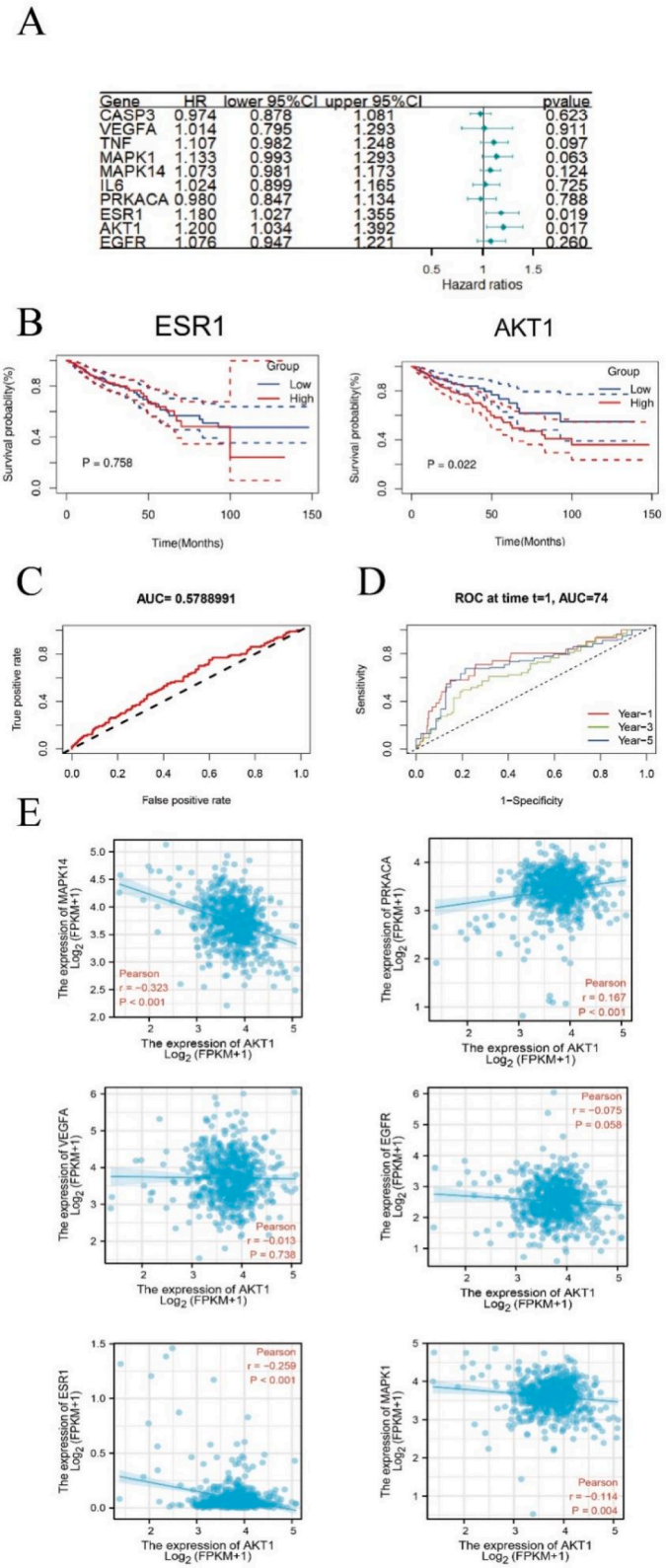

Fig. 4. The clinical correlation analysis of core gene in colorectal cancer. (A) Unigenic Cox prognostic regression analysis of network core genes. (B) Survival curves for *AKT1* and *ESR1*. (C)ROC curve for *AKT1*. (D)time- ROC curve for *AKT1*(E) Scatter plot for correlation analysis.

against CRC (Fig. 2B).

3.3. Bioinformatics analysis of the mechanism by which SQYCD exerts a therapeutic effect in CRC

We analyzed the CRC-related data in TCGA database by bioinformatics methods. The data examined were drawn from tissues from 201 cases of CRC and 342 normal cases. Ultimately, we investigated the differential expression of ten key genes between normal and tumor cells and plotted these differences in a bar graph (Fig. 3A) and a box plot (Fig. 3B). The results showed that the expression levels of *CASP3*, *TNF*, *MAP*, *MAPK14*, *PRKACA*, *ESR1*, *AKT1*, and *EGFR* were significantly higher in cancerous tissues than in normal tissues ($P < 0.05$). The expression levels of *VEGFA* and *IL6* were significantly lower in cancerous tissues than in normal tissues ($P < 0.05$).

We conducted a univariate Cox prognostic regression analysis to evaluate the prognostic importance of these genes (Fig. 4A) and found that only *ESR1* and *AKT1* might be applicable to CRC prognosis. We then plotted survival curves and discovered that only *AKT1* expression was meaningfully associated with clinical survival. Patients with CRC who express *AKT1* at high levels have lower survival rates than those expressing only low levels of this gene. Hence, *AKT1* may have a negative influence on CRC treatment outcome (Fig. 4B). The receiver operating curve (ROC) plotted for the survival characteristics had an area under the curve (AUC) of 0.578. Thus, the ROC indicated that this gene is reliably predictive (Fig. 4C). Analysis of the time-ROC disclosed that the effectiveness with which *AKT1* predicts the outcome of CRC increases over time (Fig. 4D).

We conducted a co-expression correlation study on *AKT1* and six other primary genes in the drug-target framework and generated a scatter plot (Fig. 4E). The absolute correlation between *AKT1* and *MAPK14* was 0.323, and this value was significant ($P < 0.05$). This finding suggests a potential regulatory interaction between *AKT1* and *MAPK14*.

3.4. Molecular docking simulation

Molecular docking was performed to detect the binding capacities and the modes of interaction between AKT1 and the key active components of SQYCD (quercetin, kaempferol, luteolin, β-sitosterol, taxifolin, and apigenin). In molecular docking analyses, stronger affinity between the receptor and the ligand is indicated by a value of the binding energy. Specifically, binding energies of less than −5 kcal/mol are considered to indicate favorable receptor-ligand affinity. As shown in Fig. 5, the binding energies between AKT1 and

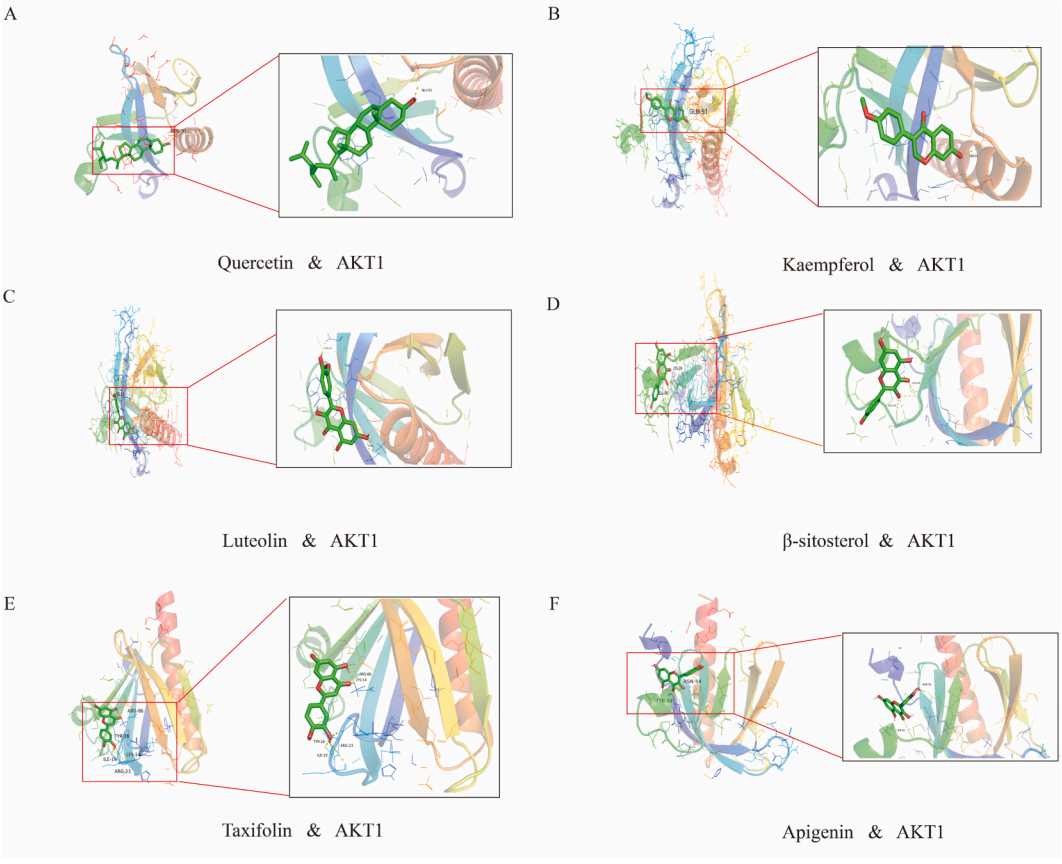

Fig. 5. Molecular docking results. (A–F) The docking of AKT1 protein with the original ligand molecules, including Quercetin, kaempferol, luteolin, β-sitosterol, taxifolin, and apigenin, resulted in certain outcomes.

β-sitosterol, luteolin, quercetin, resveratrol, myricetin, and kaempferol were calculated to be −7.0 kcal/mol, −7.0 kcal/mol, −6.4 kcal/mol, −6.2 kcal/mol, −6.3 kcal/mol, and −6.2 kcal/mol, respectively. Thus, these compounds can all be categorized as native ligands, and all six active constituents of SQYCD may interact directly with AKT1.

3.5. SQYCD inhibits the development of CRC, improves immune function, and increases tumor lymphocyte infiltration in a xenograft model

A CT-26 heterotopic subcutaneous transplantation tumor-bearing mouse model was used to test the efficacy of SQYCD in the treatment of CRC. Mice consistently administered a high dose of SQYCD (111 mg once a day; SQYC-H) over 15 d had significantly lower body weights ($P < 0.05$) than did those in the control group. In contrast, treatment with an anti-CTLA4 antibody was associated with a significantly higher average body weight ($P < 0.001$) than was treatment with control group. Relative to the control group, the tumor inhibition rates observed for the SQYC-L, SQYC-H, and anti-CTLA4 groups were 20.12 % ($P < 0.05$), 26.40 % ($P < 0.05$), and 41.91 % ($P < 0.001$), respectively.

We applied HE staining to tumor, liver, and kidney tissues to examine the antitumor efficacy of SQYCD (Fig. 6E). Staining of tumor sections from the control group revealed wide variations in cell size, chaotic cellular arrangement, and strongly staining, non-dividing oval nuclei with occasional necrotic lesions and no distinct nucleoli. However, the stained tumor sections from the SQYC-L, SQYC-H, and anti- CTLA4 groups exhibited heterogeneous cell patterns with disrupted cellular arrangements and highly irregular nuclei with abundant necrotic zonesWe evaluated the impact of SQYCD on tumor lymphocyte infiltration (Fig. 6F and G). $CD4^+$ cells was significantly higher in the SQYC-L ($P < 0.001$), SQYC-H ($P < 0.001$), and anti-CTLA4 ($P < 0.001$) groups relative to control, while $CD8^+$ cells was significantly higher in the SQYC-L ($P < 0.001$), SQYC-H ($P < 0.001$), and anti-CTLA4 ($P < 0.001$) groups than in the control group. In contrast, the protein expression of FOXP3 was lower in the SQYC-L, SQYC-H, and anti-CTLA4 groups than in the control group. While SQYCD treatment led to a dose-dependent downregulation of expression of Ki-67 compared to the control group.

3.6. SQYCD regulates lymphocytes and reduces the accumulation of Tregs in vivo

The proportions of T cells in the spleens (Fig. 7A) and tumors (Fig. 7B) were higher in the SQYC-H group than those in the control and SQYC-L groups. Furthermore, the proportions of T cells infiltrating the tumors and spleens were higher in the SQYC-H group than in the SQYC-L group (Fig. 7C).

As shown in Fig. 8C and **D**, the $CD4^+/CD8^+$ T cell ratios were significantly higher in the SQYC-L, SQYC-H, and anti-CTLA4 groups than in those of the control group ($P < 0.001$). The effect of SQYCD on the proportions of $CD4^+/CD8^+$ T cells occurred in a dose-dependent manner ($P < 0.001$).

We analyzed the proportions of $CD4^+$, $CD25^+$, and $FOXP3^+$ Tregs in the tumors to determine the ratio of Tregs on CRC. The proportions of $CD4^+$ T cells were higher in the SQYC-L, SQYC-H, and anti-CTLA4 groups than in the control group (Fig. 9A–C), while the proportions of $CD25^+$ $FOXP3^+$ cells were lower in the SQYC-L, SQYC-H groups (Fig. 9B). The frequency of $CD4^+$ $CD25^+$ $FOXP3^+$ Tregs was lower in the SQYC-L, SQYC-H groups than in the control group, especially at SQYC-H group (Fig. 9D).

3.7. SQYCD suppresses the AKT/P38α signaling pathway in tumor cells

Owing to the network and bioinformatics analyses suggested that the antitumor efficacy of SQYCD may involve the AKT/p38α signaling pathway, we investigated the effects of SQYCD on the activation of this pathway. As shown in Fig. 10, the levels of phosphorylation of both AKT and p38α and the total level of LY6G6D protein in the tumor tissues were found to be lower in the SQYC-L and SQYC-H groups than in the control group ($P < 0.001$). Similarly, immunohistochemistry assays demonstrated that LY6G6D expression was lower in the SQYC-L, SQYC-H groups than in the control group (see Fig. 10).

In cultured CT-26 cells, SQYCD treatment was found to increase the rate of apoptosis in a dose-dependent manner (Fig. 10D). The EC_{50} values for SQYCD after 24 h, 48 h, and 72 h of exposure were 1101 μg/mL, 1022 μg/mL, and 957 μg/mL, respectively. For this reason, 500 μg/mL, 1000 μg/mL, and 2000 μg/mL were used as low, moderate, and high SQYCD dosages, respectively, in further experimentation in the Western blotting analyses. According to the results of Western blotting analyses, the tumors of mice treated with the low and high doses of SQYCD displayed downregulated AKT/p38α signaling and lower LY6G6D protein expression than did those of the control group.

Stimulation of CT-26 cells with the AKT activator SC-79 was found to increase phosphorylation of both AKT and P38α; in addition, a Western blot analysis showed that this treatment increased LY6G6D protein expression (Fig. 10E). In contrast, cells treated with both SQYCD and SC-79 exhibited a decreased activation of AKT and p38α and lower LY6G6D protein expression as compared to those treated with SC-79 alone (Fig. 10F).

3.8. SQYCD alters the serum levels of inflammatory cytokines

We used ELISA to investigate the association of cytokines with the immunosuppression and immunostimulation that were observed in the mouse model. Compared to the control group, treatment with SQYCD was associated with dose-dependent increases in the serum levels of IL-6, IFN-γ, and IL-10 and a dose-dependent decrease in the serum level of IL-2 (Fig. 11).

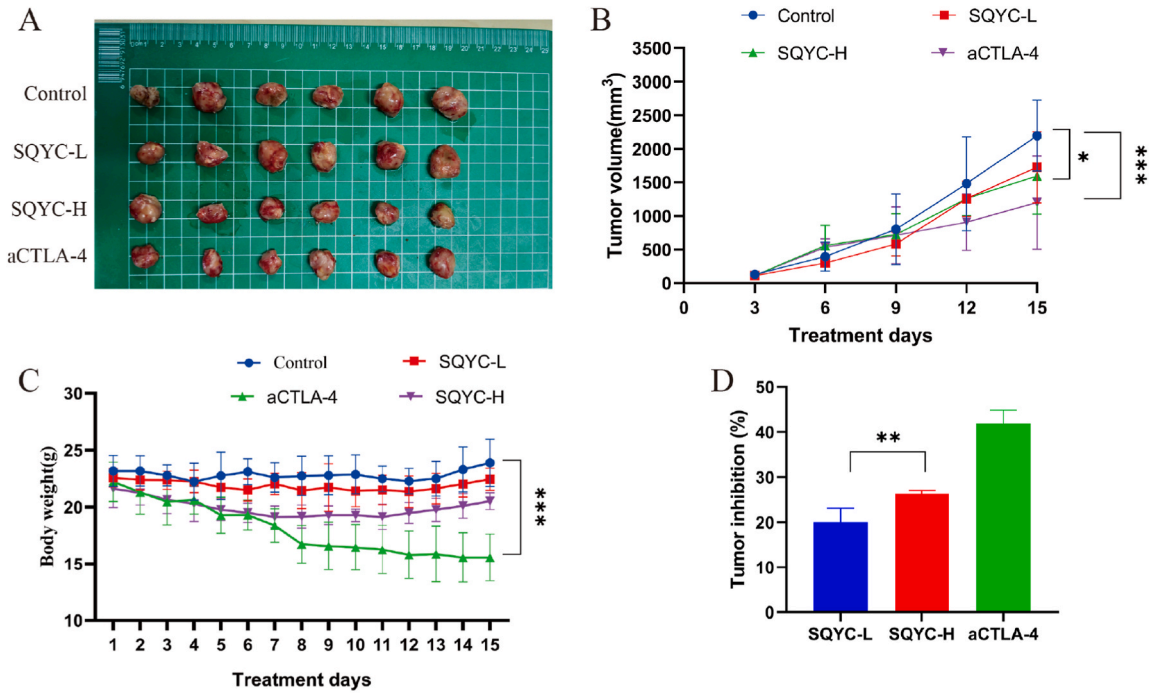

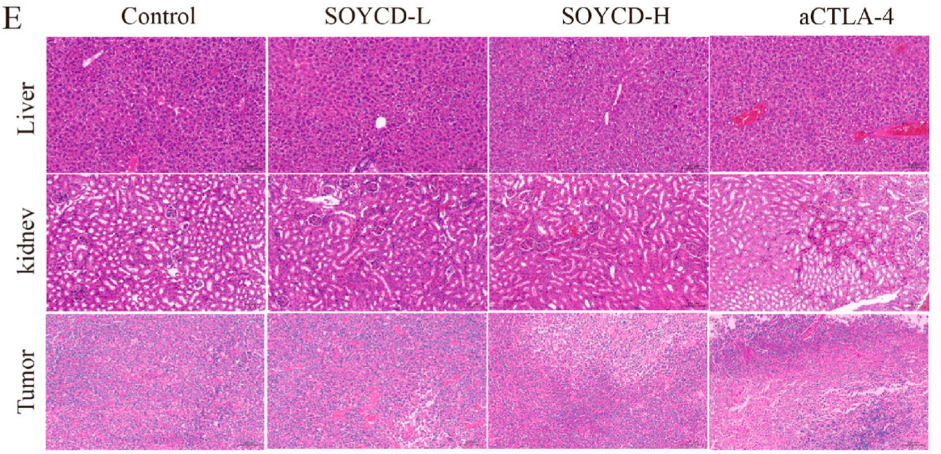

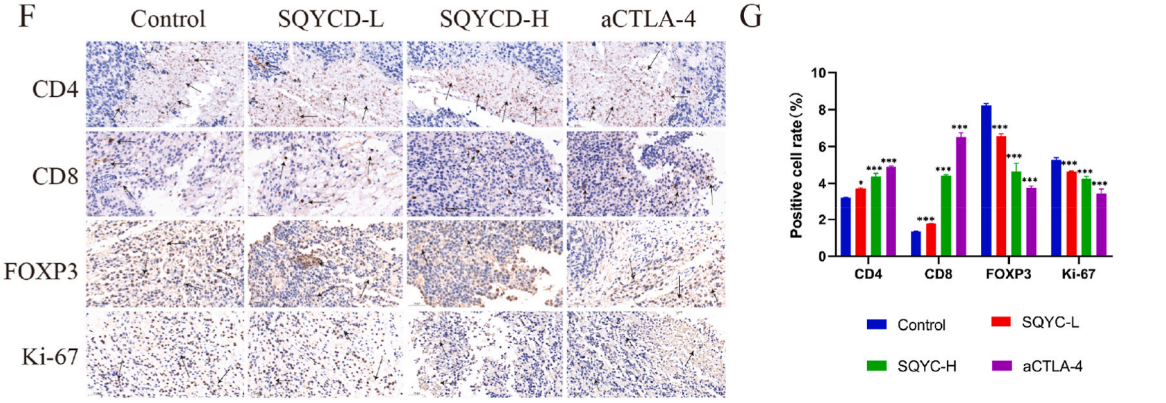

(caption on next page)

Fig. 6. Effects of SQYCD on Colorectal Cancer Xenograft and Immune Response: 24 mice were subcutaneously implanted with 1×10^6 CT-26 cells and divided into four groups: Control, SQYC-L, SQYC-H, and Anti-mouse CTLA-4.(A) Excised tumors post-treatment. (B) Tumor volume measurements every three days. (C) Daily body weight measurements. (D) Tumor Growth Inhibition Rate. (E) HE stained tumor sections. (F) Immunohistochemistry of CD4, CD8, FOXP3, and KI-67 in tumors (x 200). (G) Positive area rate. Histogram illustrating CD4, CD8, FOXP3, and KI-67 expression levels relative to the Control and SQYCD-L groups. Data represent mean ± standard deviation for six mice (*$P < 0.05$, **$P < 0.01$, ***$P < 0.001$ vs. Control group).

4. Discussion

SQYCD had previously been shown to promote the proliferation of T-lymphocytes and to improve immune function [25,26]. In the present study, the anti-tumor efficacy of SQYCD was demonstrated *in vivo* through inhibit proliferation and tumor growth in a mouse model. *In vitro*, we found that SQYCD promoted apoptosis of CT-26 cells. However, in the *vitro* study, we did not observe a clear dose-dependence of the anti-tumor effect of SQYCD; the stronger impact of SQYCD *in vivo* as compared to *in vitro* may reflect the involvement of the TME in the anti-tumor mechanism.

The present study also showed that the *in vivo* tumor-inhibitory effect of SQYCD is associated with increased numbers of $CD4^+$ and $CD8^+$ T cells and decreased numbers of Tregs in the TME. To further explore the effects of SQYCD on tumor microenvironment, we examined immune cells in the tumor tissue. We found that immunosuppressive cells, $CD4^+CD25^+FOXP3^+$ Tregs, were reduced, while $CD4^+$T cells and $CD8^+$ T cells were increased by SQYCD treatment. Next, we verified that the similar changes occurred at the level of effector or immunosuppressive cytokines. The level of IL-6 and IL-10 was reduced, while that IL-2 was increased in the tumor microenvironment by SQYCD treatment. These results indicated that the antitumor effects of SQYCD on CRC were caused not only by inhibiting cell proliferation and inducing apoptosis of tumor cells but also in part by reversing the immunosuppressive tumor microenvironment. *in vivo*, These effects were associated with the downregulation AKT/P38α signaling pathway consequently, decrease the expression of the downstream protein LY6G6D. The involvement of the AKT pathway was corroborated with vitro experiments in which AKT gonist SC-79 (prevent AKT membrane translocation and allowing phosphorylation by upstream kinases in the cytosol) selectively upregulated both the activation of AKT and p38α and the expression of LY6G6D. Taken together, these results indicate that the immunotherapeutic activity of SQYCD occurs through the targeting of the AKT/P38α/LY6G6D signaling axis, augmenting the abundance of $CD4^+$ and $CD8^+$ T cells, and diminishing the Treg ratio.

The principal ingredients of SQYCD are extracts from *Panax ginseng* and *Astragalus membranaceus,* which have been demonstrated to exert immunostimulatory and anticancer effects [36–38]. A previous study suggested that SQYCD increases the proportions of $CD4^+$ and $CD8^+$ T cells within the TME [26]. The results of the present research also demonstrated that SQYCD reduced the Treg ratio in the TME and inhibited CT-26 tumor growth in a mouse xenograft model, and high doses of SQYCD were required to directly kill CT-26 tumor cells *in vitro*. Thus, we conclude that the antitumor efficacy of SQYCD does not involve the direct inhibition of CRC cell proliferation but instead, SQYCD suppresses CRC tumor growth mainly by modulating the TME.

Evidence has suggested important roles for Tregs in mediating tumor immunity [27,28]. For example, mutations in the Treg biomarker forkhead box P3 (FOXP3) can cause severe immune dysregulation in humans and mice, and transient or moderate depletion of Tregs may impede or hinder tumor progression [29]. Patients with CRC typically present with high Treg cell titers. However, a low abundance of Tregs within CRC tumors is predictive of a favorable prognosis, and the administration of immunotherapy to inhibit Treg recruitment may be a viable treatment approach in the context of CRC. The present study empirically confirmed that SQYCD modulates the TME and reduces the Tregs ratio, supporting the importance of this decoction in cancer treatments.

Previous studies indicated that the p38α-MAPK signaling pathway affects CRC progression by altering CRC cell proliferation and viability [30,31]. AKT may control tumor proliferation and immunity as it is a regulatory element upstream of p38α [14–18]. Modulations of the p38α-MAPK signaling pathway may recalibrate inflammatory responses and antitumor mechanisms [19–21]. We postulate that the AKT/P38α signaling pathway may specifically regulate antitumor immunity. Nevertheless, an earlier report suggested that activating the AKT/p38α signaling pathway may lead to increased expression of LY6G6D, which is a CRC-specific antigen that is highly expressed in MSS CRC [11]. LY6G6D is also strongly upregulated in a CRC subtype characterized by high Tregs and low dendritic cell abundance. These observations are consistent with the downregulation of certain immune checkpoint molecules such as CTLA4 and programmed cell death receptor/protein 1 (PD-1) [22,23]. We hypothesize that the AKT/p38α signaling pathway may regulate the recruitment of immunosuppressive cells within the TME by modulating LY6G6D protein expression. Moreover, we propose that SQYCD enhances antitumor immunity by downregulating LY6G6D via inhibition of the AKT/p38α signaling pathway (Fig. 12).

Cytokines, including IL-6, IL-2, IL-10, and IFN-γ, are known to modulate cancer cell growth, often fostering tumor development and progression. Furthermore, elevated levels of these cytokines are linked with poor prognoses in MSS CRC [32,33]. Emerging therapeutic strategies for MSS CRC emphasize modulating pro-inflammatory cytokine levels. The p38 MAPK is central to inflammatory responses. Among its four isoforms—p38α, p38β, p38γ, and p38δ. p38α stands out for its extensive research footprint and its integral role in the synthesis and translation of pro-inflammatory cytokines [34,35]. Our research also underscores the capacity of SQYCD to elevate IL-2 expression, concurrently reducing IFN-γ, IL-6, and IL-10 levels *in vivo*. This suggests that the therapeutic efficacy of SQYCD in MSS CRC might hinge on its modulation of pro-inflammatory cytokines via the AKT/p38α pathway.

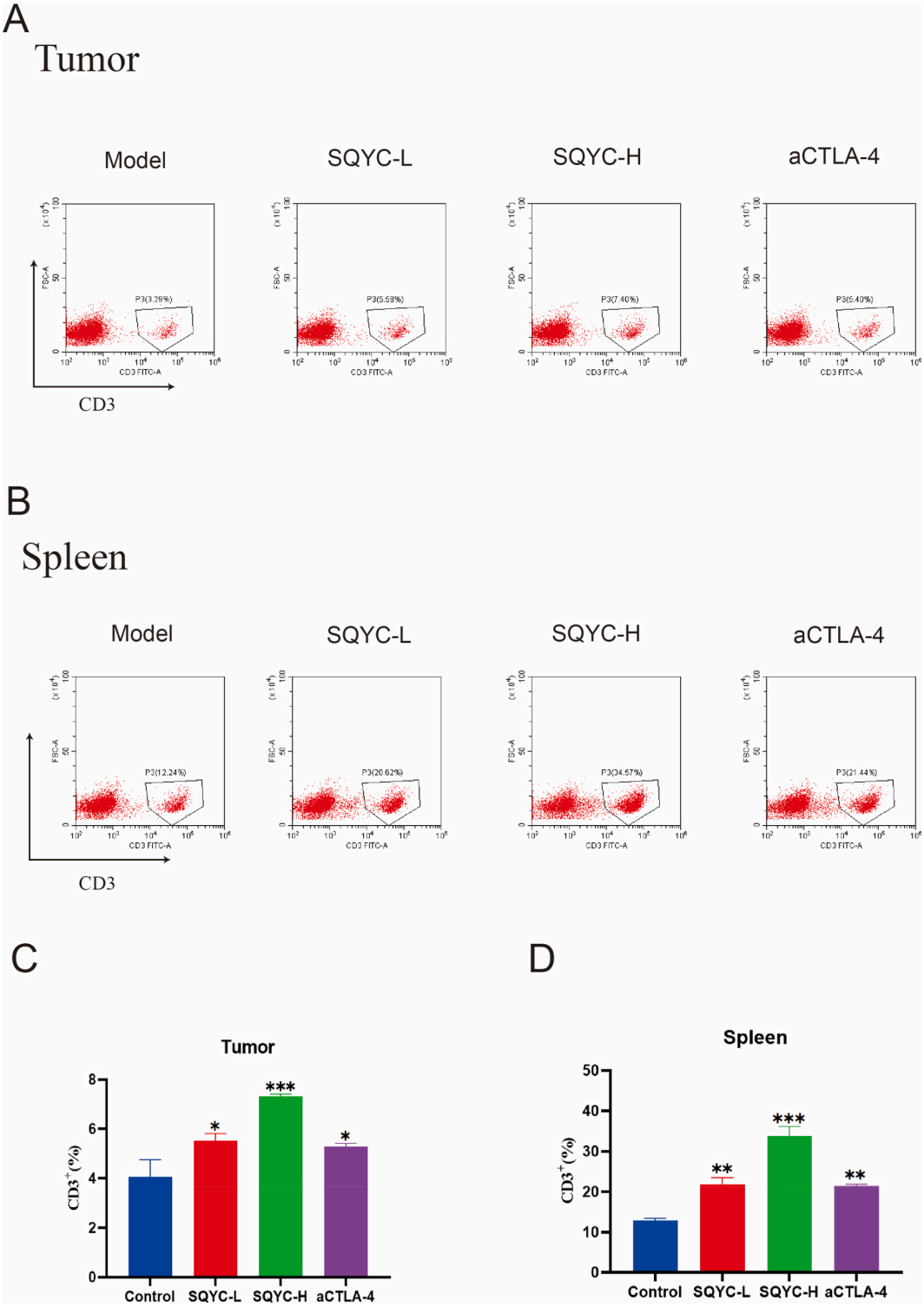

Fig. 7. SQCYD inhibits the reduction of T cells in the spleen and tumor. (A) Percentage of CD3+T cells from CT-26 tumors in each group. (B) Percentage of CD3+T cells from spleen tissue. (C) Graphs show quantifications of FACs data: Percentage of CD3+T cells from tumors. (D) Graphs show quantifications of FACs data: Percentage of CD3+T cells in splenocytes. Mean ± SD was used to express the data. The *P*-values of less than 0.05, 0.01, and 0.001 were considered statistically significant when comparing them to the Control group.

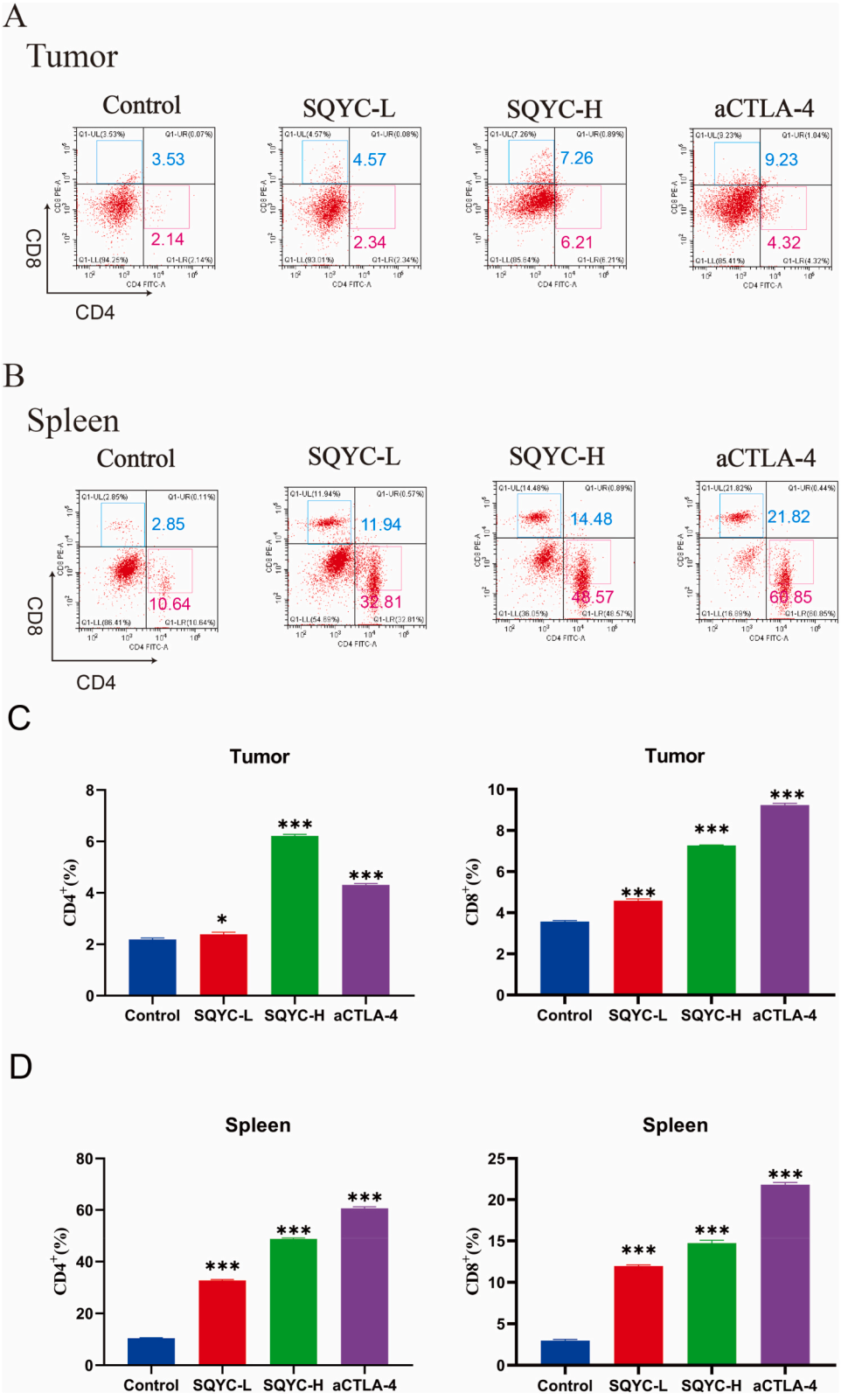

(caption on next page)

Fig. 8. SQYCD increased the CD4+/CD8+ratio in mice with colorectal cancer. (A) Percentage of CD4+/CD8+from CT-26 tumors in each group. (B) Percentage of CD4+/CD8+from splenocytes in each group. (C) Graphs show quantifications of FACs data: Percentage of CD4+/CD8+T cells from tumors. (D) Graphs show quantifications of FACs data: Percentage of CD4+/CD8+T cells from splenn. Mean ± SD was used to express the data. The *P*-values of less than 0.05, 0.01 and 0.001 were considered statistically significant when comparing them to the Control group.

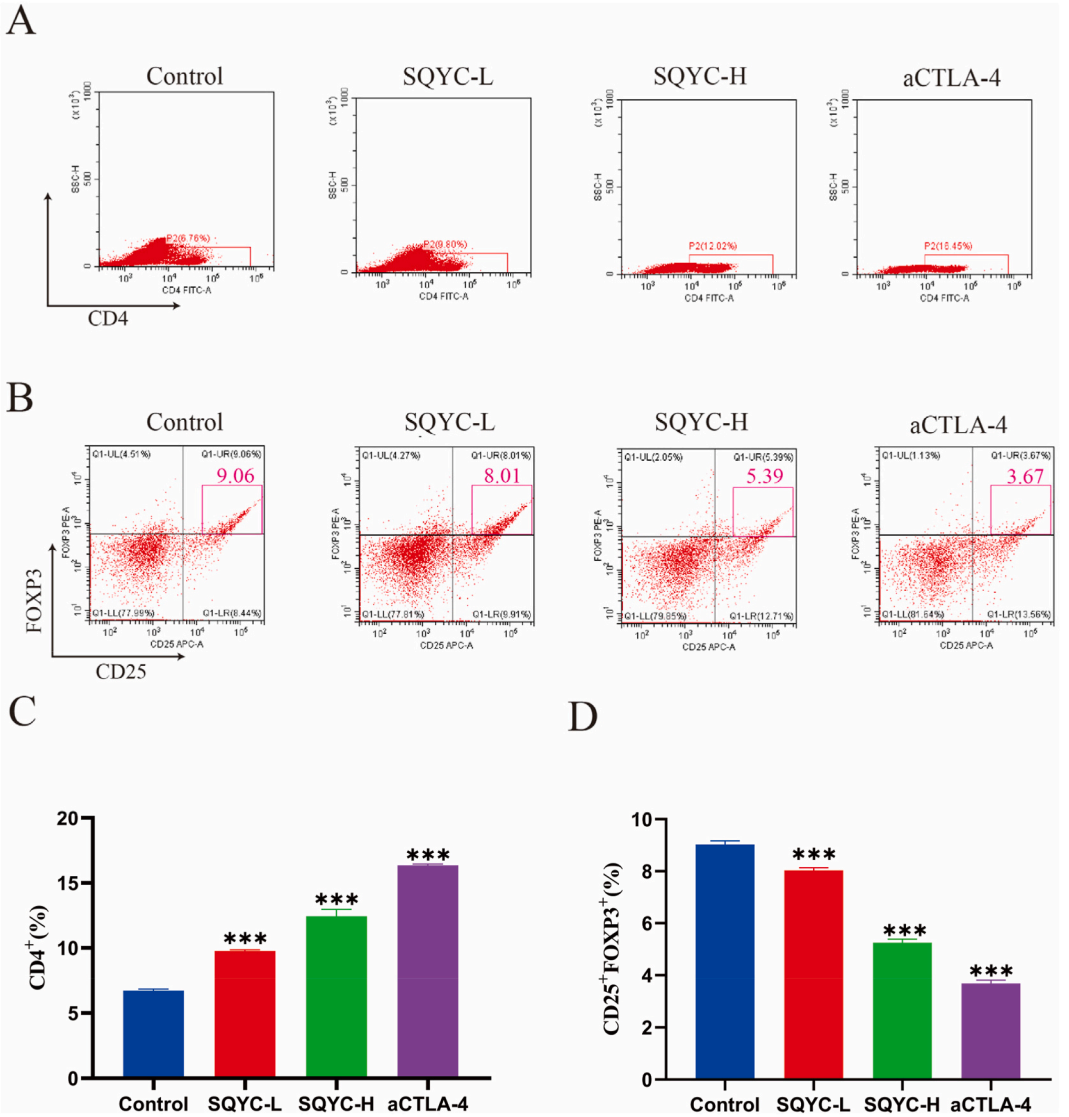

Fig. 9. SQYCD depletes Tregs in tumors. (A) Percentage of CD4+T cells from CT-26 tumors in each group. (B) CD25+FOXP3+cells were analyzed by gating on CD4+cells. (C) Graphs show quantifications of FACs data: Percentage of CD4+T cells T cells from tumors. (D) The graphs demonstrate the quantification of FACs data, specifically the percentage of $CD25^{+}$ $FOXP3^{+}$ T cells derived from tumors. The data is presented as the mean plus or minus the standard deviation. Significantly different results from the Control group are denoted as * ($P < 0.05$), ** ($P < 0.01$), or *** ($P < 0.001$).

5. Conclusion

The findings of the present study indicate that the downregulation of LY6G6D via the AKT/p38α signaling pathway and the inhibition of the aggregation and proliferation of Tregs explain the antitumor efficacy of SQYCD. The results of this work also suggest that SQYCD modulates the TME and is a promising drug in CRC treatment.

CRediT authorship contribution statement

Run Xing Luo: Writing – original draft. **Huai Liang Li:** Writing – original draft. **Yu Xiang Jia:** Writing – original draft. **Meng Gao:**

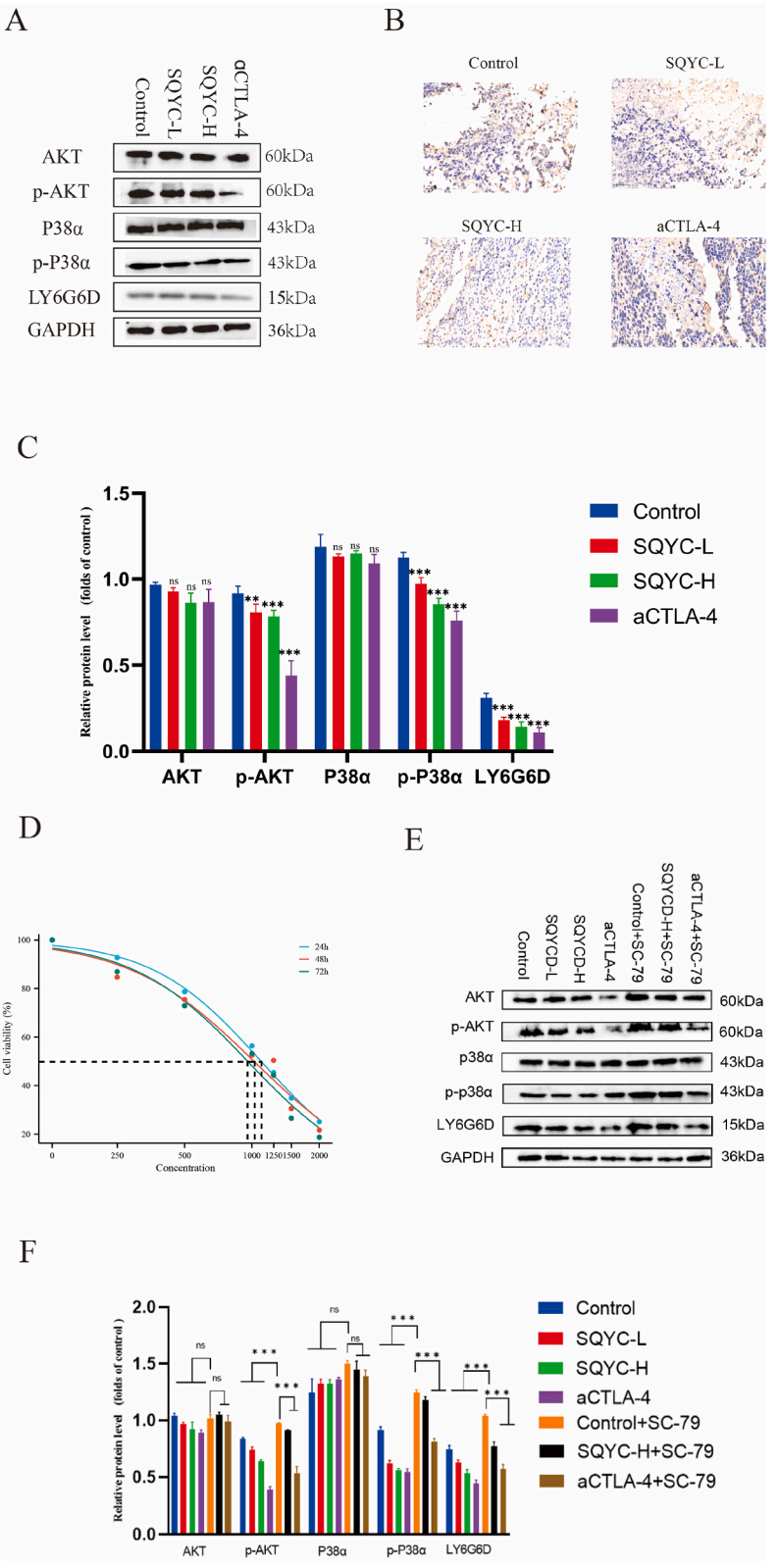

(caption on next page)

Fig. 10. SQYCD inhibited AKT/p38 signaling pathway in tumor tissues and in CT-26 cells. The images of AKT, p-AKT, P38α, and p-P38α were obtained from vitro (E) and vivo (A). (B) The expression levels of LY6G6D in tumors were detected using an immunohistochemistry assay at a magnification of × 200. (D) CCK8 analysis showed that the proliferation of CT-26 cells was inhibited in a dose-dependent manner by SQYCD treatment. Quantitative analysis was performed for *in vitro* (F) and *in vivo* (C). The values are presented as Mean ± SD for six mice. * Indicates a statistically significant difference ($P < 0.05$), ** indicates a highly significant difference ($P < 0.01$), and *** indicates an extremely significant difference ($P < 0.001$) compared to the Control group and Control + SC-79 group.

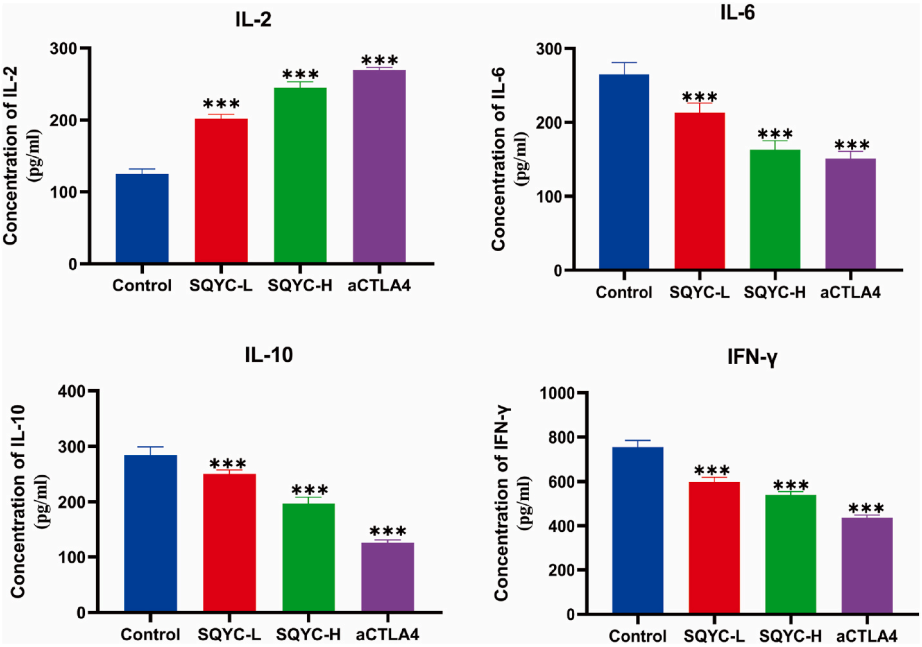

Fig. 11. ELISA analysis was conducted to measure the expressions of IL-2, IL-6, IL-10 and IFN-γ in Balb/c mice. The values are presented as Mean ± SD for six mice. * Indicates a statistically significant difference ($P < 0.05$), ** indicates a highly significant difference ($P < 0.01$), and *** indicates an extremely significant difference ($P < 0.001$) compared to the Control group.

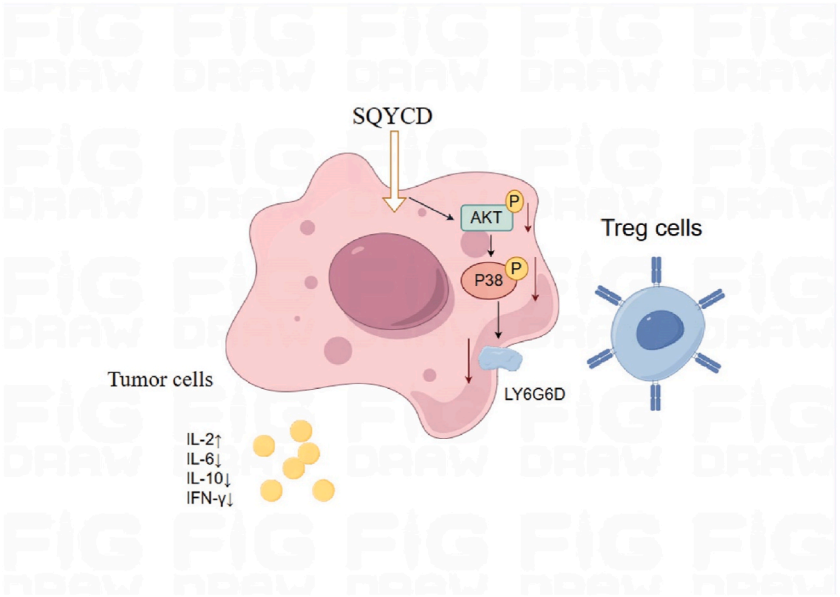

Fig. 12. The possible mechanism of SQYCD on inhibition of Tregs accumulation.

Writing – original draft. **Zhao Yang Gao:** Writing – original draft. **Yi Ji:** Methodology. **Shan Deng:** Writing – original draft. **Jie Ge Huo:** Writing – review & editing. **Jian Zhang:** Writing – review & editing. **Dong Jian Zhang:** Writing – review & editing.

Ethics Statement

Animal care and experimental procedures were approved by the Animal Ethical Committee of the Jiangsu Province Academy of Traditional Chinese Medicine endorsed all animal experiments (AEWC-20210321-287).

Data availability statement

The data used to support the findings of this study are available from the corresponding author upon reasonable request.

Funding

This work was supported by the Jiangsu Clinical Innovation Center of Digestive Cancer of Traditional Chinese Medicine (No.2021.6); the National Natural Science Foundation of China (No.82004288); and the Medical Scientific Research Key Project of Jiangsu Provincial Health Commission (No. ZD2022020).

Declaration of Competing Interest

The authors declare that there are no conflicts of interest.

Acknowledgements

The authors would like to thank all authors of references.

Appendix A. Supplementary data

Supplementary data to this article can be found online at https://doi.org/10.1016/j.heliyon.2024.e39071.

References

[1] M. Saeed, A. Shoaib, R. Kandimalla, S. Javed, A. Amaroidal, R. Gupta, F. Aqil, Microbe-based therapies for colorectal cancer: advantages and limitations, Semin. Cancer Biol. 86 (Pt 3) (2022 Nov) 652–665.
[2] X. Zhong, X. He, Y. Wang, Z. Hu, H. Huang, S. Zhao, P. Wei, D. Li, Warburg effect in colorectal cancer: the emerging roles in tumor microenvironment and therapeutic implications, J. Hematol. Oncol. 15 (1) (2022 Nov 1), 160。.
[3] D.Y. Lizardo, C. Kuang, S. Hao, J. Yu, Y. Huang, L. Zhang, Immunotherapy efficacy on mismatch repair-deficient colorectal cancer: from bench to bedside, Biochim. Biophys. Acta Rev. Canc 1874 (2) (2020 Dec) 188447.
[4] L. Chen, X. Jiang, Y. Li, Q. Zhang, Q. Li, X. Zhang, M. Zhang, Q. Yu, D. Gao, How to overcome tumor resistance to anti-PD-1/PD-L1 therapy by immunotherapy modifying the tumor microenvironment in MSS CRC, Clin Immunol 237 (2022 Apr) 108962.
[5] T. Akin Telli, G. Bregni, M. Vanhooren, R. Saude Conde, A. Hendlisz, F. Sclafani, Regorafenib in combination with immune checkpoint inhibitors for mismatch repair proficient (pMMR)/microsatellite stable (MSS) colorectal cancer, Cancer Treat Rev. 110 (2022 Nov) 102460.
[6] Z. Zheng, T. Wieder, B. Mauerer, L. Schäfer, R. Kesselring, H. Braumüller, T cells in colorectal cancer: unravelling the function of different T cell subsets in the tumor microenvironment, Int. J. Mol. Sci. 24 (14) (2023 Jul) 11673.
[7] L. Zhang, P. Romero, Metabolic control of CD8+ T cell fate decisions and anti-tumor immunity, Trends Mol. Med. 24 (1) (2018 Jan) 30–48.
[8] H. Yoshitomi, H. Ueno, Shared and distinct roles of T peripheral helper and T follicular helper cells in human diseases, Cell. Mol. Immunol. 18 (3) (2021 Mar) 523–527.
[9] T. Saito, H. Nishikawa, H. Wada, Y. Nagano, D. Sugiyama, K. Atarashi, Y. Maeda, M. Hamaguchi, N. Ohkura, E. Sato, H. Nagase, J. Nishimura, H. Yamamoto, S. Takiguchi, T. Tanoue, W. Suda, H. Morita, M. Hattori, K. Honda, M. Mori, Y. Doki, S. Sakaguchi, Two FOXP3(+) CD4(+) T cell subpopulations distinctly control the prognosis of colorectal cancers, Nat Med 22 (6) (2016 Jun) 679–684.
[10] J. Cho, W. Kuswanto, C. Benoist, D. Mathis, T cell receptor specificity drives accumulation of a reparative population of regulatory T cells within acutely injured skeletal muscle, Proc Natl Acad Sci U S A 116 (52) (2019 Dec 26) 26727–26733.
[11] L. Corrales, S. Hipp, K. Martin, N. Sabarth, I. Tirapu, K. Fuchs, B. Thaler, C. Walterskirchen, K. Bauer, M. Fabits, M. Bergmann, C. Binder, P.M. Chetta, A.B. Vogt, P.J. Adam, LY6G6D is a selectively expressed colorectal cancer antigen that can be used for targeting a therapeutic T-cell response by a T-cell engager, Front. Immunol. 13 (2022 Sep 8) 1008764.
[12] G. Giordano, P. Parcesepe, M.R. D'Andrea, L. Coppola, T. Di Raimo, A. Remo, E. Manfrin, C. Fiorini, A. Scarpa, C.A. Amoreo, F. Conciatori, M. Milella, F. P. Caruso, L. Cerulo, A. Porras, M. Pancione, JAK/Stat5-mediated subtype-specific lymphocyte antigen 6 complex, locus G6D (LY6G6D) expression drives mismatch repair proficient colorectal cancer, J. Exp. Clin. Cancer Res. 38 (1) (2019 Jan 22) 28.
[13] F.P. Caruso, M.R. D'Andrea, L. Coppola, M. Landriscina, V. Condelli, L. Cerulo, G. Giordano, A. Porras, M. Pancione, Lymphocyte antigen 6G6D-mediated modulation through p38α MAPK and DNA methylation in colorectal cancer, Cancer Cell Int. 22 (1) (2022 Aug 11) 253.
[14] M.A. Siraj, A.T. Jacobs, G.T. Tan, B. Altersolanol, A fungal tetrahydroanthraquinone, inhibits the proliferation of estrogen receptor-expressing (ER+) human breast adenocarcinoma by modulating PI3K/AKT, p38/ERK MAPK and associated signaling pathways, Chem. Biol. Interact. 359 (2022 May 25) 109916.
[15] H.T. Yeh, Y.S. Tsai, M.S. Chen, Y.Z. Li, W.C. Lin, Y.R. Lee, Y.S. Tseng, S.M. Sheu, Flavopereirine induces cell cycle arrest and apoptosis via the AKT/p38 MAPK/ERK1/2 signaling pathway in human breast cancer cells, Eur. J. Pharmacol. 863 (2019 Nov 15) 172658.
[16] D. Ge, J. Gao, L. Han, Y. Li, H.H. Liu, W.C. Yang, F. Chang, J. Liu, M. Yu, J. Zhao, Novel effects of sphingosylphosphorylcholine on the apoptosis of breast cancer via autophagy/AKT/p38 and JNK signaling, J. Cell. Physiol. 234 (7) (2019 Jul) 11451–11462.

[17] T. Xuan, D. Wang, J. Lv, Z. Pan, J. Fang, Y. Xiang, H. Cheng, X. Wang, X. Guo, Downregulation of Cypher induces apoptosis in cardiomyocytes via Akt/p38 MAPK signaling pathway, Int. J. Med. Sci. 17 (15) (2020 Aug 27) 2328–2337.
[18] J.S. Seok, C.H. Jeong, M.C. Petriello, H.G. Seo, H. Yoo, K. Hong, S.G. Han, Piperlongumine decreases cell proliferation and the expression of cell cycle-associated proteins by inhibiting Akt pathway in human lung cancer cells, Food Chem. Toxicol. 111 (2018 Jan) 9–18.
[19] J. Taieb, M. Svrcek, R. Cohen, D. Basile, D. Tougeron, J.M. Phelip, Deficient mismatch repair/microsatellite unstable colorectal cancer: diagnosis, prognosis and treatment, Eur. J. Cancer 175 (2022 Nov) 136–157.
[20] W.W. Ho, I.L. Gomes-Santos, S. Aoki, M. Datta, K. Kawaguchi, N.P. Talele, S. Roberge, J. Ren, H. Liu, I.X. Chen, P. Andersson, S. Chatterjee, A.S. Kumar, Z. Amoozgar, Q. Zhang, P. Huang, M.R. Ng, V.P. Chauhan, L. Xu, D.G. Duda, J.W. Clark, M.J. Pittet, D. Fukumura, R.K. Jain, Dendritic cell paucity in mismatch repair-proficient colorectal cancer liver metastases limits immune checkpoint blockade efficacy, Proc Natl Acad Sci U S A 118 (45) (2021 Nov 9) e2105323118.
[21] H. Xu, K. Van der Jeught, Z. Zhou, L. Zhang, T. Yu, Y. Sun, Y. Li, C. Wan, K.M. So, D. Liu, M. Frieden, Y. Fang, A.L. Mosley, X. He, X. Zhang, G.E. Sandusky, Y. Liu, S.O. Meroueh, C. Zhang, A.B. Wijeratne, C. Huang, G. Ji, X. Lu, Atractylenolide I enhances responsiveness to immune checkpoint blockade therapy by activating tumor antigen presentation, J. Clin. Invest. 131 (10) (2021 May 17) e146832.
[22] R. Zappasodi, I. Serganova, I.J. Cohen, M. Maeda, M. Shindo, Y. Senbabaoglu, M.J. Watson, A. Leftin, R. Maniyar, S. Verma, M. Lubin, M. Ko, M.M. Mane, H. Zhong, C. Liu, A. Ghosh, M. Abu-Akeel, E. Ackerstaff, J.A. Koutcher, P.C. Ho, G.M. Delgoffe, R. Blasberg, J.D. Wolchok, T. Merghoub, CTLA-4 blockade drives loss of Treg stability in glycolysis-low tumours, Nature 591 (7851) (2021 Mar) 652–658.
[23] S. Li, R. Na, X. Li, Y. Zhang, T. Zheng, Targeting interleukin-17 enhances tumor response to immune checkpoint inhibitors in colorectal cancer, Biochim. Biophys. Acta Rev. Canc 1877 (4) (2022 Jul) 188758.
[24] Z. Zhong, C.T. Vong, F. Chen, H. Tan, C. Zhang, N. Wang, L. Cui, Y. Wang, Y. Feng, Immunomodulatory potential of natural products from herbal medicines as immune checkpoints inhibitors: helping to fight against cancer via multiple targets, Med. Res. Rev. 42 (3) (2022 May) 1246–1279.
[25] L. Li, M. Fang, X. Wang, J. Huo, Clinical observation of Fufangchangtai decoction combined with FOLFOX4 regimen for postoperative colorectal cancers, Chin. Ger. J. Clin. Oncol. 10 (4) (2011) 225–227.
[26] Y.F. Ding, S. Zhang, X.N. Wang, M.Q. Shen, Fufang Changtai's effect on the caspase-3 way of apoptosis in colon cancer cell SW480, Journal of Nanjing University of Traditional Chinese Medicine 27 (4) (2011) 346–350.
[27] Y. Togashi, K. Shitara, H. Nishikawa, Regulatory T cells in cancer immunosuppression - implications for anticancer therapy, Nat. Rev. Clin. Oncol. 16 (6) (2019 Jun) 356–371.
[28] C. Tay, A. Tanaka, S. Sakaguchi, Tumor-infiltrating regulatory T cells as targets of cancer immunotherapy, Cancer Cell 41 (3) (2023 Mar 13) 450–465.
[29] J.B. Wing, A. Tanaka, S. Sakaguchi, Human FOXP3+ regulatory T cell heterogeneity and function in autoimmunity and cancer, Immunity 50 (2) (2019 Feb 19) 302–316.
[30] J. Yuan, X. Dong, J. Yap, J. Hu, The MAPK and AMPK signalings: interplay and implication in targeted cancer therapy, J. Hematol. Oncol. 13 (1) (2020 Aug 17) 113.
[31] Y. Xu, N. Li, R. Xiang, P. Sun, Emerging roles of the p38 MAPK and PI3K/AKT/mTOR pathways in oncogene-induced senescence, Trends Biochem. Sci. 39 (6) (2014 Jun) 268–276.
[32] Z. Zhu, P. Parikh, H. Zhao, N.T. Givens, D.B. Beck, C.M. Willson, Q. Bai, M.R. Wakefield, Y. Fang, Targeting immunometabolism of neoplasms by interleukins: a promising immunotherapeutic strategy for cancer treatment, Cancer Lett. 518 (2021 Oct 10) 94–101.
[33] A. Zlotnik, Chemokines in neoplastic progression, Semin. Cancer Biol. 14 (3) (2004 Jun) 181–185.
[34] H.B. Park, K.H. Baek, E3 ligases and deubiquitinating enzymes regulating the MAPK signaling pathway in cancers, Biochim. Biophys. Acta Rev. Canc 1877 (3) (2022 May) 188736.
[35] I. Peluso, N.S. Yarla, R. Ambra, G. Pastore, G. Perry, MAPK signalling pathway in cancers: olive products as cancer preventive and therapeutic agents, Semin. Cancer Biol. 56 (2019 Jun) 185–195.
[36] S. Xiaodan, C. Ying, Role of ginsenoside Rh2 in tumor therapy and tumor microenvironment immunomodulation, Biomed. Pharmacother. 156 (2022 Dec) 113912.
[37] J. Huang, D. Liu, Y. Wang, L. Liu, J. Li, J. Yuan, Z. Jiang, Z. Jiang, W.W. Hsiao, H. Liu, I. Khan, Y. Xie, J. Wu, Y. Xie, Y. Zhang, Y. Fu, J. Liao, W. Wang, H. Lai, A. Shi, J. Cai, L. Luo, R. Li, X. Yao, X. Fan, Q. Wu, Z. Liu, P. Yan, J. Lu, M. Yang, L. Wang, Y. Cao, H. Wei, E.L. Leung, Ginseng polysaccharides alter the gut microbiota and kynurenine/tryptophan ratio, potentiating the antitumour effect of antiprogrammed cell death 1/programmed cell death ligand 1 (anti-PD-1/PD-L1) immunotherapy, Gut 71 (4) (2022 Apr) 734–745.
[38] D. Wang, Q. Cui, Y.J. Yang, A.Q. Liu, G. Zhang, J.C. Yu, Application of dendritic cells in tumor immunotherapy and progress in the mechanism of anti-tumor effect of Astragalus polysaccharide (APS) modulating dendritic cells: a review, Biomed. Pharmacother. 155 (2022 Nov) 113541.
[39] L. Li, Randomized, Double-Blind Controlled Study of Fufangchangtai Granule in the Treatment of Colon Cancer, Nanjing University of Chinese Medicine, Nanjing, 2019. Doctoral Dissertation.